Ultrasound in Medicine & Biology 50 (2024) 358–363

Contents lists available at ScienceDirect

Ultrasound in Medicine & Biology

journal homepage: www.elsevier.com/locate/ultrasmedbio

Original Contribution

Automated 3-D Ultrasound Elastography of the Breast: An *In Vivo* Validation Study

Gijs A.G.M. Hendriks [a], Chuan Chen [a], Ritse Mann [b], Hendrik H.G. Hansen [a], Chris L. de Korte [a,c,*]

[a] *Medical Ultrasound Imaging Center, Department of Medical Imaging, Radboud University Medical Center, Nijmegen, The Netherlands*
[b] *Breast Imaging Group, Department of Medical Imaging, Radboud University Medical Center, Nijmegen, The Netherlands*
[c] *Physics and Fluids Group, Faculty of Science and Technology, University of Twente, Enschede, The Netherlands*

ARTICLE INFO

Keywords:
Ultrasound
Elastography
Characterization
Screening
Breast cancer
Automated breast volume scanner

Objective: Studies have indicated that adding 2-D quasi-static elastography to B-mode ultrasound imaging improved the specificity for malignant lesion detection, as malignant lesions are often stiffer (increased strain ratio) compared with benign lesions. This method is limited by its user dependency and so unsuitable for breast screening. To overcome this limitation, we implemented quasi-static elastography in an automated breast volume scanner (ABVS), which is an operator-independent 3-D ultrasound system and is especially useful for screening women with dense breasts. The study aim was to investigate if 3-D quasi-static elastography implemented in a clinically used ABVS can discriminate between benign and malignant breast lesions.
Methods: Volumetric breast ultrasound radiofrequency data sets of 82 patients were acquired before and after automated transducer lifting. Lesions were annotated and strain was calculated using an in-house-developed strain algorithm. Two strain ratio types were calculated per lesion: using axial and maximal principal strain (*i.e.,* strain in dominant direction).
Results: Forty-four lesions were detected: 9 carcinomas, 23 cysts and 12 other benign lesions. A significant difference was found between malignant (median: 1.7, range: [1.0–3.2]) and benign (1.0, [0.6–1.9]) using maximal principal strain ratios. Axial strain ratio did not reveal a significant difference between benign (0.6, [−12.7 to 4.9]) and malignant lesions (0.8, [−3.5 to 5.1]).
Conclusion: Three-dimensional strain imaging was successfully implemented on a clinically used ABVS to obtain, visualize and analyze *in vivo* strain images in three dimensions. Results revealed that maximal principal strain ratios are significantly increased in malignant compared with benign lesions.

Introduction

In 2020, more than 500,000 women were diagnosed with breast cancer and 141,765 women died of breast cancer in Europe [1]. In 1990, breast cancer screening programs were introduced in The Netherlands to reduce mortality. Studies indicated that annual screening before diagnosis reduced breast cancer-specific mortality [2]. In those screening programs, mammography was commonly used as a detection method. In mammography, the breast is compressed between two transparent plates and a 2-D low-dose X-ray projection of the breast is obtained. The disadvantage of mammography is the use of radiation and its limited sensitivity in women with dense breasts [3]. Dense breasts contain a relatively large amount of fibroglandular tissue, which is more often present in younger women. This tissue can mask possible cancers in the 2-D projections acquired by mammography.

Ultrasound imaging is an inexpensive alternative or supplement to mammography in breast cancer detection, especially in women with dense breasts [4]. The main disadvantage of ultrasound imaging is that exams are performed using a hand-held transducer, making screening highly operator dependent, time consuming and thus still expensive. To overcome this limitation, automated breast volume scanners (ABVSs) were introduced. These ultrasound devices consist of a large linear transducer (154 mm footprint) that is mechanically moved over the breast while acquiring ultrasound data. Next, 3-D ultrasound volumes of the breast are reconstructed, and B-mode images can be visualized and inspected in every requested plane (*e.g.,* coronal, sagittal or transverse). Wojcinski et al. [5] investigated the clinical performance of the ABVS and reported that ABVS screening had high sensitivity and fair interobserver agreement. They also reported that the specificity of ABVS screening was low, resulting in high recall rates, additional follow-up exams and unnecessary biopsies.

The addition of quasi-static elastography [6] to B-mode imaging is aimed at increasing the specificity of ABVS through assessment of the mechanical properties of tissues and lesions. In elastography, ultrasound data are acquired before and after an induced deformation of the tissue. Next, tissue displacements and strains are calculated by advanced cross-

* Corresponding author. Medical Ultrasound Imaging Center, Department of Medical Imaging, Radboud University Medical Center, PO Box 9010, 6500 HB, Nijmegen, The Netherlands.
E-mail address: Chris.deKorte@radboudumc.nl (C.L. de Korte).

https://doi.org/10.1016/j.ultrasmedbio.2023.11.006
Received 12 April 2023; Revised 23 October 2023; Accepted 9 November 2023

correlation and strain estimation algorithms [7–9]. The estimated strains, often axial strains, are used as surrogate measures for stiffness. As carcinomas of non-specific type (NST) have increased Young's moduli (~500 kPa at 20% pre-compression) compared with benign tissues (20, 60 and 200 kPa in fatty, glandular and fibrous tissue, respectively) [10], malignant lesions will strain less than benign lesions when the same deformation is applied. Therefore, malignant and benign lesions can in theory be discriminated by measuring the deformation along the beam (axial strain) when deforming the tissue by lowering or lifting the transducer membrane. Thomas et al. [11] reported that the specificity in differentiating between benign and malignant lesions increased from 56% in B-mode imaging to 89% in quasi-static elastography using hand-held transducers. In a previous study, we determined that it was feasible to implement quasi-static elastography in an ABVS-mimicking device, to visualize strain in 3-D and to detect stiff lesions in a breast phantom [12].

The aim of this study was to verify whether it was feasible to discriminate between benign and malignant lesions in a prospective study. Therefore, quasi-static 3-D elastography was implemented in a clinically used ABVS (Acuson S2000, Siemens Healthineers, Issaquah, WA, USA) using the same protocol described in Hendriks et al. [12] except for the ultra-fast plane-wave acquisitions as these were not available in this commercial scanner. Consequently, we used conventional focused line-by-line acquisitions with one focal spot and without the use of compounding, which implied the acquisition time was relatively long: ~15 s per volume. Therefore, the patient was allowed to breathe between the two volumetric scans before and after applying different levels of deformation as required for elastography. Because of the breathing, which possibly induced deformation in directions other than the axial direction, we also investigated the discriminative power of the maximal principal strain as an alternative measure for lesion stiffness next to the axial strain. The maximal principal strain can be derived from the 3-D strain tensor and represents the largest pure strain direction without shear.

Methods

The protocol was approved by the local institutional ethics committee (CMO Radboudumc, Project No. CMO 2016-2692). All participants gave written informed consent. From July 2017 until October 2019, 87 patients participated in this study. Adult women (≥18 y) who were scheduled for a mammogram or ultrasound breast exam at Radboud University Medical Center (Radboudumc, Nijmegen, the Netherlands) for breast cancer screening (asymptomatic patients) or after being referred by their general practitioner or healthcare professional (symptomatic patients) were included. Women who were pregnant or lactating were excluded.

Data collection

The data collection and elastography calculation steps are summarized in Figure 1. All measurements were executed using an ABVS ultrasound system (Acuson S2000) with an ultrasound research interface (URI) to enable storage of beam-formed ultrasound radiofrequency (RF) data. The ABVS transducer (14L5BV) was positioned on top of the breast while the patient was in supine position similar to that in a regular scan. If the patient had a known lesion (*e.g.,* palpable lesion or by previous exam), the ABVS transducer was positioned such that the lesion was centered within the field of view (FOV); otherwise, the transducer was positioned to cover the largest part of the breast. Furthermore, the transducer's footprint was always oriented parallel to the floor and perpendicular to the lifting direction. When required (for views other than true anterior–posterior), a pillow was placed behind the patient's back to rotate her upper body such that the rib cage was also as parallel as possible to the transducer's footprint to maximize surface contact. After positioning, volumetric ultrasound RF data were obtained twice, using ABVS scans without any post-processing (center frequency of 8.9 MHz, single focus at 14 mm depth). Each RF data set contained 3168 samples (sampled at 40 MHz) for 512 image lines for 316 elevational planes. The line density was 3.3 lines/mm, and the elevational plane distance was 0.5 mm. Patients were asked to hold their breath during each scan (~15 s). Between the two scans, the transducer was automatically lifted (~1 mm) to induce a differential axial deformation.

As ground truth, the diagnostic results of the regular breast exam were used, which included mammography and ultrasound exams evaluated by experienced radiologists and biopsy results if available. Those exam results were used as reference for annotation of the obtained stacked B-mode and strain images as described in the next section and to classify the lesions.

Elastography calculations

The initially obtained volumetric RF-data set was converted to stacked B-mode images by demodulation and logarithmic conversion. The lesion was annotated manually frame by frame. The strains measured in a sphere inside the lesion and in a box surrounding the lesion served as signal and reference strains, respectively, to calculate strain ratios as described later. The sphere covered 75% of the annotated lesion mean radius; the box covered a rectangular area at 7.5 mm distance from the lesion border, excluding the lesion and its 2.5 mm surrounding tissue.

Displacements and strains were estimated as in Hendriks et al. [12], who reported that 3-D tracking outperformed 2-D tracking in volumetric frame-by-frame scanning. In short, displacements were calculated by 3-D coarse-to-fine cross-correlation (cc) in four cc-iterations using downsampled demodulated RF data in the first two iterations and RF data in the remaining iterations. In each iteration, kernel and search window sizes were decreased (Table 1) and the cc function (ccf) peak position of the previous iteration was used as offset. The kernel overlap was 50%, 70% and 70% in the axial, lateral and elevational directions,

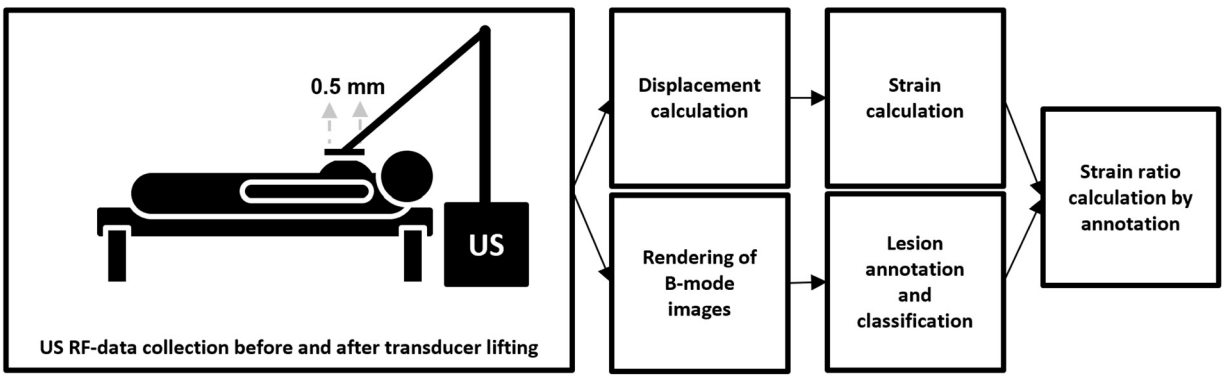

Figure 1. Summary of the data collection and post-processing steps to obtain elastography results (axial and maximal principal strain ratios). RF, radiofrequency; US, ultrasound.

Table 1
Kernel, window and filter settings of the coarse-to-fine cross-correlation algorithm

Iteration	Kernel (mm)	Window (mm)	Filter (mm)
1. Env[a]	3.6 × 2.1 × 2.5	7.2 × 5.1 × 7.5	20 × 6.6 × 11
2. Env[a]	1.8 × 1.5 × 2.5	3.6 × 2.1 × 3.5	10 × 3.3 × 5.5
3. RF	0.92 × 1.5 × 2.5	1.8 × 2.1 × 3.5	3.2 × 2.1 × 3.5

Env, enveloped data; RF, radiofrequency data.
[a] Envelope data are axially downsampled (factor 11) to decrease calculation times and to approximate a point spread function-based grid.

respectively. Displacements were median filtered after each iteration, and subsample displacements were calculated by 3-D spline interpolation of the ccf peak after the final iteration. An 11 × 3 × 3-point 3-D least-squares strain estimator [7] was used to derive the 3-D strain tensor values. Strain ratios were determined by calculating the ratio between mean strain in the signal (sphere inside the annotated lesion) and reference region (box around lesion). Strain ratios were required to quantify strain and to correct for differences in induced strain by breathing artifacts between scans, and in applied strain by different breast cup size. To calculate the stain ratios, the maximal principal or axial strain component of the 3-D strain tensor was used. The maximal principal strain component was calculated by selecting the largest absolute eigenvalue of the strain tensor, which represents the strain in the pure dominant strain direction.

Statistical analysis

Statistical analysis was executed in SPSS (SPSS Statistics Version 25, IBM, Armonk, NY). The Mann–Whitney *U*-test was used to compare the axial and maximal principal strain ratios between the benign (abscess, AD, IP, FA, PT) and malignant lesions (DCIS, NST, ILC, MC) with a significance level (p) of 0.05.

Results

Eighty-seven female patients were included; 5 of these patients were excluded because of a failed scan or declined participation. Of the resulting 82 women, 39 did not reveal any abnormalities or had focal abnormalities that turned out to be normal tissue (*i.e.,* fat lobes, or palpable lesions by locally dense glandular or fibroglandular tissue). The remaining group of 43 women revealed 44 abnormalities. On the basis of regular clinical evaluation (including biopsy when appropriate), these were caused by 4 invasive carcinomas of no-special type (NST), 4 ductal carcinomas *in situ* (DCIS), 1 invasive lobular carcinoma (ILC), 1 mucinous carcinoma, 23 cysts, 8 fibro-adenomas (FA), 1 intraductal papilloma (IP), 1 adenoma (AD), 1 abscess and 1 benign phyllodes tumor (PT). One DCIS was excluded as it was detected by MRI but was not visible on ultrasound. In one patient, an FA and AD were detected in the same breast. Patient age varied between 21 and 77 y with a median of 49 y. The numbers of women with Volpara breast densities A, B, C and D were 1, 6, 9 and 15, respectively, determined automatically with Volpara breast density software using the raw mammography images. Ten women younger than 30 y did not undergo mammography, and so breast density was not determined. In 2 women, the breast density could not be calculated. Strain estimates inside cysts were inaccurate because of their hypo-echogenic characteristics. These lesions were not further analyzed in this study. An overview of all included lesion types, corresponding breast densities and strain ratios can be found in Table 2.

Two typical B-mode and strain ratio images of an NST and FA are visualized in Figures 2 and 3, respectively, in the coronal, transverse and sagittal views. In the strain ratio results (Fig. 2d–f), the area within and around the NST had increased principal strain ratios (3–6) whereas the surrounding tissue had ratios around 1. The maximal principal strain ratios of the FA (Fig. 3d–f) were similar to those of the surrounding breast tissue (0–2). The axial and maximal principal strain ratios for all annotated lesions are summarized in Figure 4 and Table 2. The axial strain ratio (Fig. 4a) ranged from −12.7 to 4.9 (median = 0.6) and from −3.5 to 5.1 (median = 0.8) for benign and malignant lesions,

Table 2
Results for all patients

Lesion type	Classification[a]	Breast density[b]	Axial strain ratio	Principal strain ratio
Abscess	Benign	C	4.473	0.785
AD	Benign	D	−0.424	0.762
FA	Benign	D	0.880	0.637
FA	Benign	<30 y[c]	2.258	1.097
FA	Benign	<30 y[c]	−1.096	0.664
FA	Benign	D	−0.214	0.652
FA	Benign	<30 y[c]	−6.922	1.806
FA	Benign	D	0.616	1.918
FA	Benign	<30 y[c]	0.615	1.311
FA	Benign	D	−12.729	0.856
IP	Benign	C	4.926	1.341
PT	Benign	<30 y[c]	1.149	1.078
ILC	Malignant	B	1.596	2.761
DCIS	Malignant	N/A[c]	0.798	1.454
DCIS	Malignant	D	1.103	1.013
DCIS	Malignant	C	0.090	1.684
MC	Malignant	D	3.726	2.985
NST	Malignant	B	−3.518	2.733
NST	Malignant	C	−0.546	3.219
NST	Malignant	D	0.557	1.161
NST	Malignant	B	5.060	1.346

AD, adenoma; DCIS, ductal carcinoma *in situ*; FA, fibro-adenoma; ILC, invasive lobular carcinoma; IP, intraductal papilloma; MC, mucinous carcinoma; N/A, not available; NST, invasive carcinomas of non-specific type; PT, benign phyllodes tumor.
[a] The classifications malignant lesion and benign lesion were used as two independent groups in the Mann–Whitney *U*-test.
[b] Volpara breast density score obtained by mammography.
[c] Mammography, and thus the breast density score, was not available because of referral from other hospital (N/A) or because the woman was younger than 30 y of age.

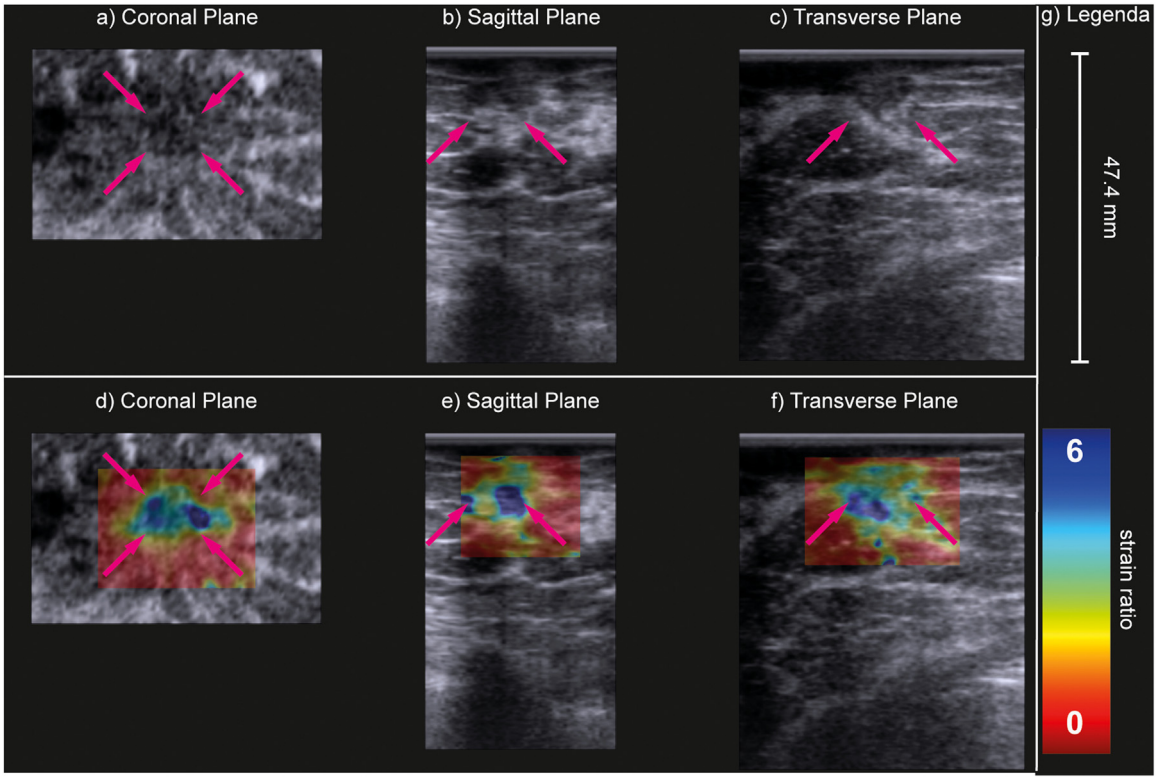

Figure 2. B-mode (a–c) and strain ratio (d–f) images of a carcinoma of unknown type in the coronal (a, d), sagittal (b, e) and transverse (c, f) planes. In the strain images (d–f), the maximal principal strain ratios are superimposed on the B-mode images of the top row. The *purple arrows* indicate the lesion.

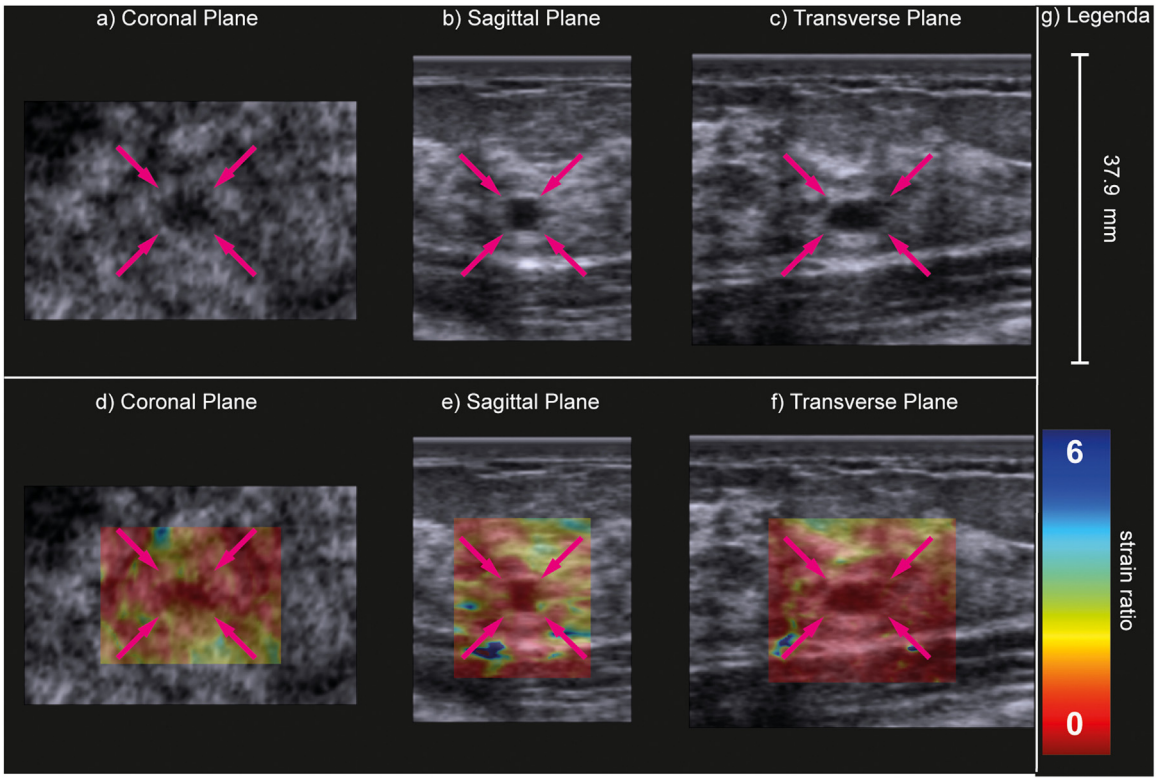

Figure 3. B-mode (a–c) and strain ratio (d–f) images of a fibro-adenoma in the coronal (a, d), sagittal (b, e) and transverse (c, f) planes. In the strain images (d–f), the maximal principal strain ratios are superimposed on the B-mode images of the top row. The *purple arrows* indicate the lesion.

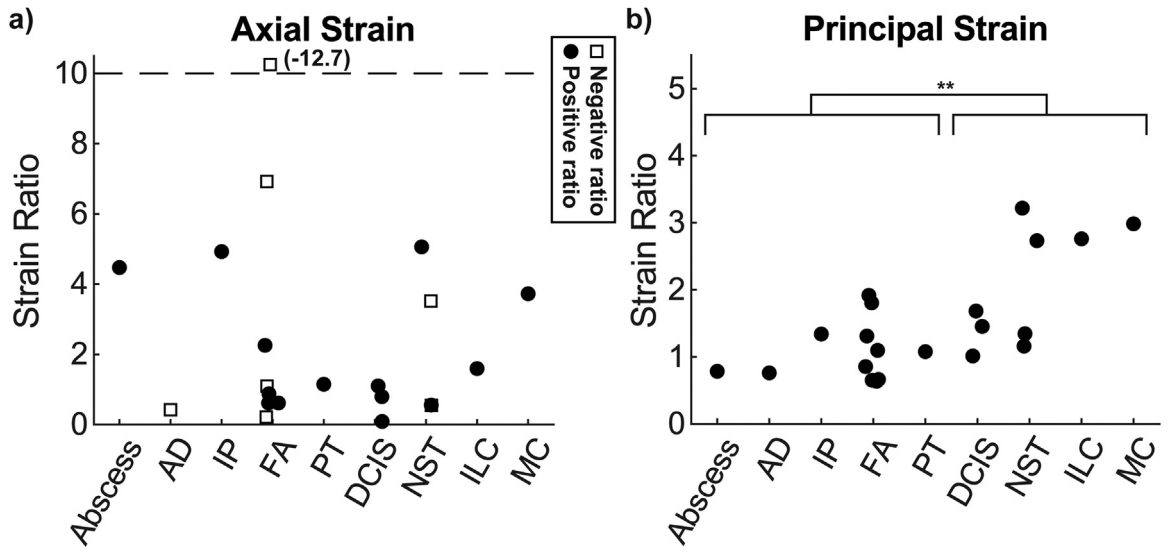

Figure 4. Scatterplots of the median axial (a) and maximal principal (b) strain ratios in each lesion. *Squares* represent negative strain ratios (*i.e.,* signs of the median strain in the lesion and background are opposite). **Significant difference in principal strain ratios ($p = 0.007$) between the benign (abscess, AD, IP, FA, PT) and malignant (DCIS, NST, ILC, MC) lesions. The difference in axial strain ratio was not significant ($p = 0.558$). The Mann–Whitney *U*-test was used to compare two independent benign and malignant groups. Eleven lesions were classified as benign: 1 abscess, 1 adenoma (AD), 1 intraductal papilloma (IP), 8 fibro-adenomas (AD) and 1 benign phyllodes tumor (PT). Nine lesions were classified as malignant: 4 invasive carcinomas of nonspecific type (NST), 3 ductal carcinomas *in situ* (DCIS), 1 invasive lobular carcinoma (ILC) and 1 mucinous carcinoma (MC). Twenty-three cysts were excluded from analysis as strain estimates inside cysts were inaccurate because of the hypoechogenic characteristics of the cysts. More details on the lesion types included can be found in Table 2.

respectively. Negative axial strain ratios indicated that the axial strain in the lesion was opposite in sign to that of the reference area. On evaluation of the maximal principal strain components (Fig. 4b), it was observed that the malignant lesions had a median strain ratio between 1.0 and 3.2 (median = 1.7), which was significantly increased ($p = 0.007$) compared with benign lesions with a ratio between 0.6 and 1.9 (median = 1.7).

Discussion

Figure 4b illustrates that the maximal principal strain ratios were increased significantly in malignant lesions as compared to benign lesions which included FA. Principal strains were derived as they represented the strain in the pure dominant strain direction. This direction can deviate from the axial direction, in which the deformation was induced, because of breathing artifacts and the curved rib cage, which is not always completely parallel to the surface of the ABVS transducer pod. The sign of the axial strain ratio was negative in some lesions (Fig. 4a, Table 2), and most of those lesions had a high axial strain ratio (>6) or a ratio close to zero. In those lesions, the axial strain direction was not the main strain direction because of changing boundary conditions (*i.e.,* rib case shape, motion). Consequently, the axial strain became small and close to zero. The estimated strain ratio can become negative when the signs of the strain are opposite in the reference and lesion area. This often occurred when the strain was around zero in one of the areas and flipped sign because of some small inaccuracies in strain calculations. The ratios became close to zero or large if the strain was close to zero in the reference or lesion area, respectively. This can be overcome by using the maximal principal strain in which the dominant strain direction was evaluated instead of the axial direction.

The maximal principal strain ratios of malignant compared with benign lesions were consistent with results in the literature. Stachs et al. [13] reported that malignant lesions had axial strain ratios of 3.04 ± 0.90 (mean ± standard deviation), whereas benign lesions had ratios around 1.91 ± 0.75. Furthermore, NSTs appeared larger on the strain images (Fig. 2d–f) than on the B-mode images (Fig. 2a–c), which was also consistent with the literature [14]. The PT had a strain ratio value of 1.1 (Fig. 4b, Table 2) similar to that of the FA (0.6–1.9), which was expected because PT and FA are both fibro-epithelial tumour types [15]. The DCIS lesions had strain ratios in the same range as benign lesions. This suggests equal stiffness, which was also reported for ultrasound shear wave imaging [16] and was explained by the relatively small size of DCIS lesions (<15 mm) and the usually more diffuse growth pattern of these lesions. The difference in ratio was still significant between benign and malignant lesions including DCIS. On inspection of Table 2, it seems that breast density and strain ratio did not correlate per lesion type (*e.g.,* NST had maximal principal strain ratios of 1.2, 1.3, 2.7 and 3.2 with breast densities D, B, B and C, respectively), suggesting the independence of breast density. The next step is to extend this study to a larger population to further investigate breast density–strain dependency and to verify feasibility and eventually to a large screening population to evaluate clinical performance. Furthermore, the reproducibility and repeatability of the method have to be verified.

The maximal principal strain ratio was used as surrogate measure for stiffness because the direction of deformation may be altered by boundary condition, which might result in off-axis deformation: the breast tissue is deformed between the paddle containing the transducer and the rib cage, and these might not be aligned in parallel. In this study, the maximal principal strain component was defined as the component with the largest absolute median value in the calculated strain area around the lesion. Consequently, the first principal strain component was used if mainly stretching occurred, and the third component if mainly compression occurred. Visual inspection of the eigenvector directions corresponding to the principal strains revealed that directions were mostly consistent within the volume.

To induce deformation, the transducer was lifted automatically between acquisitions. Alternatively, breathing can be used instead of lifting to induce deformation. The first data set can be collected during a breath hold with partly full lungs, and the second data set, with empty lungs. The advantage is that breathing is controlled during the scans although it will remain difficult to control the amount of deformation, and it is unlikely that this is effective for lesions located very laterally in the breast as motion caused by breathing in that area is limited. Large

deformations and strain can reduce the accuracy of displacement estimates because of decorrelation. Ultra-fast ultrasound imaging (plane-wave imaging) can be a solution to prevent breathing artifacts as this technique allows high acquisition rates, and so both acquisitions (before and after transducer lifting) can be performed within one breath hold. Unfortunately, ultra-fast acquisitions are currently not available in most commercially available ultrasound systems.

The full 3-D strain tensor is required to calculate principal strain components [17]. The disadvantage is that this implies that also contributing in the calculation are the lateral and elevational displacement estimates, which are of reduced accuracy compared with axial displacement especially because phase information was lacking. Angular displacement compounding (ADC) can be implemented to improve lateral displacement estimates [18]. In ADC, displacements are estimated along different large beam-steering angles that include phase information, and these estimates are used to derive the horizontal (lateral) displacements. In the ABVS, ADC cannot be used to improve the accuracy of elevational displacement estimates as beam steering is not possible in the elevational direction. A disadvantage of ADC is that more acquisitions are required, the acquisition time increases (*e.g.,* by a factor of 3 when using three beam-steering angles) and so the RF data cannot be recorded within one breath hold. Again, ultra-fast ultrasound imaging can overcome this limitation of ADC. Another benefit of ADC may be that insonification under the nipple area can be improved by the use of large beam-steering angles.

To quantify strain, strain ratios were calculated to correct for differences in applied strain between patients caused by breathing and different breast sizes. Therefore, the lesions had to be annotated manually, which was time consuming. Manual annotation may also be replaced by automated segmentation of the tissue layers. Strain quantification can also be performed by normalization of the strain data by obtaining the applied pressure (*e.g.,* by sensors on the transducer surface). An alternative for strain ratios is the Tsukuba scoring system [19] in which the strain pattern is used to classify lesions. This scoring method requires manual inspection of the strain images although computer-aided diagnosis systems (*e.g.,* machine or deep learning algorithms) may contribute to automate classification in future applications. An advantage of that scoring system is that cysts can also be evaluated as they reveal a typical strain pattern, so-called blue–green–red (BGR) sign, in strain images, which is basically a strain artifact caused by the hypo-echogenic area inside cysts. In this study, cysts were not evaluated because of this artifact resulting in unreliable estimates of the strain inside them.

Conclusion

We successfully implemented and executed 3-D strain imaging on a clinical ultrasound breast-volume scanner and obtained, visualized and analyzed *in-vivo* strain images in three dimensions. The results indicate that maximal principal strain ratios were significantly increased in malignant lesions compared with benign lesions including fibroadenoma.

Data availability statement

Clinical ultrasound radiofrequency data sets might be available on request for collaborative works. A data sharing agreement needs to be arranged between the mutual centers.

Conflict of interest

The authors declare no competing interests.

Acknowledgments

This research is supported by Siemens Healthineers and by the Dutch Technology Foundation STW (Project 13290), which is part of the Netherlands Organization for Scientific Research (NWO) and is partly funded by the Ministry of Economic Affairs.

The authors thank Chi-Yin Lee, Andy Milkowski and co-workers of Siemens Healthineers for their technical support, and the sonographers and student assistants of the department of Medical Imaging of the Radboudumc Nijmegen for their clinical support.

References

[1] Sung H, Ferlay J, Siegel RL, Laversanne M, Soerjomataram I, Jemal A, et al. Global Cancer Statistics 2020: GLOBOCAN estimates of incidence and mortality worldwide for 36 cancers in 185 countries. CA Cancer J Clin 2021;71:209–49.
[2] Myers ER, Moorman P, Gierisch JM, Havrilesky LJ, Grimm LJ, Ghate S, et al. Benefits and harms of breast cancer screening: a systematic review. JAMA 2015;314:1615–34.
[3] Kolb TM, Lichy J, Newhouse JH. Comparison of the performance of screening mammography, physical examination, and breast US and evaluation of factors that influence them: an analysis of 27,825 patient evaluations. Radiology 2002;225:165–75.
[4] Corsetti V, Houssami N, Ghirardi M, Ferrari A, Speziani M, Bellarosa S, et al. Evidence of the effect of adjunct ultrasound screening in women with mammography-negative dense breasts: interval breast cancers at 1 year follow-up. Eur J Cancer 2011;47:1021–6.
[5] Wojcinski S, Gyapong S, Farrokh A, Soergel P, Hillemanns P, Degenhardt F. Diagnostic performance and inter-observer concordance in lesion detection with the automated breast volume scanner (ABVS). BMC Med Imaging 2013;13:36.
[6] Ophir J, Céspedes I, Ponnekanti H, Yazdi Y, Li X. Elastography: a quantitative method for imaging the elasticity of biological tissues. Ultrason Imaging 1991;13:111–34.
[7] Kallel F, Ophir J. A least-squares strain estimator for elastography. Ultrason Imaging 1997;19:195–208.
[8] Chen H, Shi H, Varghese T. Improvement of elastographic displacement estimation using a two-step cross-correlation method. Ultrasound Med Biol 2007;33:48–56.
[9] Lopata RG, Nillesen MM, Hansen HH, Gerrits IH, Thijssen JM, de Korte CL. Performance evaluation of methods for two-dimensional displacement and strain estimation using ultrasound radio frequency data. Ultrasound Med Biol 2009;35:796–812.
[10] Krouskop TA, Wheeler TM, Kallel F, Garra BS, Hall T. Elastic moduli of breast and prostate tissues under compression. Ultrason Imaging 1998;20:260–74.
[11] Thomas A, Degenhardt F, Farrokh A, Wojcinski S, Slowinski T, Fischer T. Significant differentiation of focal breast lesions: calculation of strain ratio in breast sonoelastography. Acad Radiol 2010;17:558–63.
[12] Hendriks GA, Hollander B, Menssen J, Milkowski A, Hansen HH, de Korte CL. Automated 3D ultrasound elastography of the breast: a phantom validation study. Phys Med Biol 2016;61:2665–79.
[13] Stachs A, Hartmann S, Stubert J, Dieterich M, Martin A, Kundt G, et al. Differentiating between malignant and benign breast masses: factors limiting sonoelastographic strain ratio. Ultraschall Med 2013;34:131–6.
[14] Garra BS, Céspedes EI, Ophir J, Spratt SR, Zuurbier RA, Magnant CM, et al. Elastography of breast lesions: initial clinical results. Radiology 1997;202:79–86.
[15] Azzopardi JG, Chepick OF, Hartmann WH, Jafarey NA, Llombart-Bosch A, Ozzello L, et al. The World Health Organization Histological Typing of Breast Tumors. Am J Clin Pathol 1982;78:806–16.
[16] Vinnicombe SJ, Whelehan P, Thomson K, McLean D, Purdie CA, Jordan LB, et al. What are the characteristics of breast cancers misclassified as benign by quantitative ultrasound shear wave elastography? Eur Radiol 2014;24:921–6.
[17] Hendriks G, Chen C, Hansen HHG, de Korte CL. 3-D single breath-hold shear strain estimation for improved breast lesion detection and classification in automated volumetric ultrasound scanners. IEEE Trans Ultrason Ferroelectr Freq Control 2018;65:1590–9.
[18] Hendriks G, Hansen HHG, De Korte CL, Chen C. Optimization of transmission and reconstruction parameters in angular displacement compounding using plane wave ultrasound. Phys Med Biol 2020;65:085007.
[19] Itoh A, Ueno E, Tohno E, Kamma H, Takahashi H, Shiina T, et al. Breast disease: clinical application of US elastography for diagnosis. Radiology 2006;239:341–50.